Binding energies of excitons trapped by ionized donors in semiconductors

A. S. dos Santos,[1] Mauro Masili,[2] and J. J. De Groote[3]
[1]*Instituto de Física de São Carlos, Universidade de São Paulo–USP, Caixa Postal 369, 13 560-970 São Carlos, SP, Brazil*
[2]*Associação de Escolas Reunidas–ASSER, Rua Miguel Petroni 5111, 13 563-470 São Carlos, SP, Brazil*
[3]*Instituto de Química de Araraquara, Universidade Estadual Paulista–UNESP, Caixa Postal 355, 14 801-970 Araraquara, SP, Brazil*
(Received 8 May 2001; published 26 October 2001)

Using the hyperspherical adiabatic approach in a coupled-channel calculation, we present precise binding energies of excitons trapped by impurity donors in semiconductors within the effective-mass approximation. Energies for such three-body systems are presented as a function of the relative electron-hole mass σ in the range $1 \leqslant 1/\sigma \leqslant 6$, where the Born-Oppenheimer approach is not efficiently applicable. The hyperspherical approach leads to precise energies using the intuitive picture of potential curves and nonadiabatic couplings in an *ab initio* procedure. We also present an estimation for a critical value of $\sigma\,(\sigma_{\rm crit})$ for which no bound state can be found. Comparisons are given with results of prior work by other authors.

DOI: 10.1103/PhysRevB.64.195210 PACS number(s): 71.35.−y, 71.15.−m

I. INTRODUCTION

The existence of bound exciton complexes in semiconductors was predicted by Lampert[1] in 1958, and since then such systems have been theoretically and experimentally studied.[2–12] Within the effective-mass approximation in which effective masses are attributed to both electron (m_e) and hole (m_h), interacting through a Coulombian field in the semiconductor, Thomas and Hopfield[4] used a Born-Oppenheimer approach to perform qualitative calculation of binding energies of such complexes in the presence of an impurity donor. These systems behave as three-body complexes, and the possibility of binding together depends on the electron-hole mass proportion. Thus the system can be analyzed as a function of the ratio $\sigma = m_e/m_h$. For small values of σ the hole is much more massive than the electron, and the system behaves as a diatomic molecule. As σ becomes larger, the number of vibrational binding energies decreases up to the point where there is only one stable state, with a very small binding energy. For values of σ above a critical point called *critical mass* $(\sigma_{\rm crit})$, the hole is no longer bound to the electron-impurity ''atom.''

The analysis of these D^+X complexes for light holes is very difficult due to the very small dissociation energy. The Born-Oppenheimer approach is inappropriate since the distance between the hole and the impurity cannot be considered an adiabatic variable. The independent particle approximation is also difficult to apply due to the hole-impurity repulsive potential field, whose correlation effects are important. The variational approach, however, has been used by many authors[5,7–9] with precise results, but it lacks the intuitive description and visibility of the methods previously cited. An alternative approach, i.e., the hyperspherical (HS) adiabatic method, has been used with efficiency to deal with systems with light holes.[13–15] This method brings together the high precision aspect of the variational calculation with the potential curves intuitive picture. The HS treatment is based on the use of hyperspherical coordinates, which are defined to correlate the radial variables of the electron (r_e) and hole (r_h) in an analogous way as the two-dimensional Cartesian coordinates are related to the polar coordinates. For the D^+X systems the HS coordinates are the hyperradius R and the hyperangle α, defined as $R^2 = m_e r_e^2 + m_h r_h^2$ and $\tan\alpha = \sqrt{\sigma} r_e / r_h$. The hyperradius is the unique radial variable of the rewritten Schrödinger equation, while the hyperangle α is compact. The original spherical variables are not changed by the coordinate transformation. The main advantage of these new coordinates is that R is a good adiabatic variable since it is related to the particles moment of inertia, which changes slowly (adiabatically) compared to α. The adiabatic approach using the HS coordinates is developed similarly to the Born-Oppenheimer approximation for diatomic molecules. For fixed values of R, taken as a parameter, the angular part of the HS Schrödinger equation is solved. The outcome is a set of potential curves and channel functions which are the input for the obtaining of the nonadiabatic couplings; both potential curves and couplings are further used in the solution of the radial equations. The procedure is *ab initio* and its simplest radial approximation, where all the nonadiabatic terms are neglected, is good enough to give the position of the binding energy within a 1% error. Moreover, as the couplings are introduced into the radial equations the calculated energy approaches the exact value in a systematic and controllable way.[14–19]

The HS adiabatic approach was introduced in atomic calculations by Macek[20] in the late 1960s for the qualitative study of resonant states of the helium atom. Since then it has evolved to become a very precise method,[21–25,16–18] allowing the calculation of energies of the ground state up to highly excited states[16,17] of atomic systems, as well as of general three-body problems.[24–27] The method has also been applied to four-body systems.[28–37] The application of this method for bound excitons without the nonadiabatic couplings has given good qualitative results.[13,14] Recently[15] a HS coupled-channel calculation has been performed, proving that this method also leads to very accurate results, with precision comparable to the variational energy values found in literature. Those results have been achieved for excitons bound to donor impurities in CdS $[1/\sigma = 5$ (Ref. 9)] and ZnSe $[1/\sigma = 6$ (Ref. 8)] semiconductors with a nonadiabatic calculation coupling only four hyperspherical radial channels.[15]

The aim of this paper is to extend the coupled-channel

hyperspherical adiabatic approach to excitons bound to singly ionized impurity donors within the range $1 \leqslant 1/\sigma \leqslant 6$, which corresponds to systems with a unique binding energy, where the Born-Oppenheimer approach is not adequate. This range comprehends excitons for a large variety of semiconductors, like ZnSe ($1/\sigma=6$), CdS ($1/\sigma=5$), and CdSe [$1/\sigma=4.23$ (Ref. 12)]; it also allows a study of the system behavior as σ approaches the region of critical mass, where the limit for the binding of these three-body systems is approached. There does not exist a good consensus among different calculations by others since it is necessary extremely precise wave functions in the region of the critical mass.

In Sec. II we outline the theoretical aspects of the hyperspherical adiabatic approach and discuss the corresponding equations. In Sec. III the angular equation is solved to obtain the potential curves and channel functions, which are used for the calculation of the nonadiabatic couplings. In Sec. IV the results are discussed and Sec. V presents the conclusions.

II. HYPERSPHERICAL ADIABATIC APPROACH

Excitonic complexes within the effective-mass approximation are represented by an electron and a hole with effective mass m_e and m_h, respectively, interacting through a Coulombian field and composing a hydrogenlike atom. In the presence of an impurity donor the system may form a bound three-body complex with the spectral characteristics provided by the proportion between the electron and hole effective masses. The Hamiltonian for such system in spherical coordinates is given by

$$\hat{H} = -\frac{\hbar^2}{2m_e}\nabla_e^2 - \frac{\hbar^2}{2m_h}\nabla_h^2 - \frac{Ze^2}{\epsilon r_e} + \frac{Ze^2}{\epsilon r_h} - \frac{e^2}{\epsilon|\vec{r}_e - \vec{r}_h|}, \quad (1)$$

where ϵ is the dielectric constant of the semiconductor, Z is the effective atomic number of the impurity, and $\vec{r}_e$ and $\vec{r}_h$ are the radial coordinates of the electron and the hole with respect to the impurity, taken as the center of mass.

The properties of these systems can be analyzed in terms of σ. As the value of σ decreases, the ground-state energy becomes lower and the vibrational levels are present, in a similar way as the diatomic spectral lines. As the hole effective mass approaches the value of the electronic effective mass, the number of vibrational states decreases up to the point where σ reaches σ_{crit} and no binding energy is observed. There is not an agreement in literature for the value of σ_{crit}. One of the reasons for the disparities is that the hole wave function is very delocalized, requiring very precise numerical methods.

The hyperspherical coordinates are defined in terms of the radial spherical coordinates as

$$R = \sqrt{m_e r_e^2 + m_h r_h^2} \quad (2)$$

and

$$\alpha = \tan^{-1}\left(\sqrt{\sigma}\,\frac{r_e}{r_h}\right). \quad (3)$$

This relation maps the set of six coordinates of the system $\{r_e, r_h, \theta_e, \phi_e, \theta_h, \phi_h\}$ into a set with five angular coordinates and only one radial coordinate, $\{R, \alpha, \theta_e, \phi_e, \theta_h, \phi_h\}$ (the spherical angles are not changed by the introduction of the hyperspherical coordinates). Even for more complex systems with more particles, the hyperspherical coordinates are constructed in such a way that they generate only one radial coordinate.[38] This is very useful for the numerical development of the Schrödinger equation. Using arbitrary units ($\hbar = m_e = e^2/\epsilon = 1$) the Schrödinger equation rewritten in hyperspherical coordinates is given by

$$\left(\frac{\partial^2}{\partial R^2} + \frac{\hat{U}(R;\Omega) + 1/4}{R^2} + 2E\right)(R^{5/2}\sin\alpha\cos\alpha)^{-1}\Psi(R;\Omega) = 0. \quad (4)$$

The angular operator $\hat{U}(R;\Omega)$ contains all the angular variables, i.e.,

$$\hat{U}(R;\Omega) = \frac{\partial^2}{\partial\alpha^2} - \frac{\hat{L}_e^2}{\sin^2\alpha} - \frac{\hat{L}_h^2}{\cos^2\alpha} - R\hat{V}(\Omega), \quad (5)$$

where Ω denotes the set of angular coordinates $\{\alpha, \theta_e, \phi_e, \theta_h, \phi_h\}$ and

$$\hat{V}(\Omega) = -\frac{2Z}{\sin\alpha} + \frac{2Z}{\sqrt{\sigma}\cos\alpha} - \frac{2}{\sqrt{\sin^2\alpha + \sigma\cos^2\alpha - \sqrt{\sigma}\sin 2\alpha\cos\theta_{eh}}} \quad (6)$$

contains the terms of the interaction potential, where $\cos\theta_{eh} = \hat{\mathbf{r}}_e \cdot \hat{\mathbf{r}}_h$. The operator $\hat{U}(R;\Omega)$ can be written in a compact form as a function of the Casimir operator of the group $O(6)$,

$$\hat{U}(R;\Omega) = C_2[O(6)] - R\hat{V}(\Omega), \quad (7)$$

which is useful in the classification scheme of the states.[25] This equation shows explicitly the simple linear dependence of the angular operator with respect to the hyperradius, which suggests the adiabatic separation of the total wave function,

$$\Psi(R;\Omega) = \sum_\mu F_\mu(R)\Phi_\mu(R;\Omega), \quad (8)$$

where the basis set is formed by eigenstates $\Phi_\mu(R;\Omega)$ of the angular operator, i.e.,

$$\hat{U}(R;\Omega)\Phi_\mu(R;\Omega) = U_\mu(R)\Phi_\mu(R;\Omega). \quad (9)$$

The eigenvalues and eigenstates are obtained for each discretized value of R. The hyperspherical adiabatic approach proceeds by initially solving the eigenvalue Eq. (9). The eigenvalues $U_\mu(R)$ are the potential curves and the eigenfunctions $\Phi_\mu(R;\Omega)$ are called angular channel functions, where the index μ represents collectively the set of quantum num-

bers $\{n,l_e,l_h\}$ of the solution at $R=0$.[20] Substituting expansion (8) into the Schrödinger equation, using the angular eigenvalue Eq. (9) and projecting into the basis set $\{\Phi_\mu(R;\Omega)\}$, the following set of coupled radial equations is obtained:

$$\left(\frac{d^2}{dR^2}+\frac{U_\mu(R)+1/4}{R^2}+2E\right)F_\mu(R) + \sum_\nu \left(2P_{\mu\nu}(R)\frac{d}{dR}+Q_{\mu\nu}(R)\right)F_\nu(R) = 0. \tag{10}$$

The couplings of this set of radial equations are the nonadiabatic couplings, namely

$$P_{\mu\nu}(R)=\left\langle \Phi_\mu \left| \frac{d}{dR} \right| \Phi_\nu \right\rangle \tag{11}$$

and

$$Q_{\mu\nu}(R)=\left\langle \Phi_\mu \left| \frac{d^2}{dR^2} \right| \Phi_\nu \right\rangle. \tag{12}$$

Equation (10) is an infinite coupled set of equations for the radial amplitudes, which must be truncated in practical calculations.

At this point one of the fundamental reasons for the use of the hyperspherical adiabatic approach (HAA) can be discussed. The exact energy E_{exact} of the system is systematically closer to the energy obtained by the solution of the truncated coupled equations as the number of couplings increases. This is the coupled adiabatic approximation (CAA). Following the variational principle, this behavior determines an upper bound energy for the exact value. Now, unlike the variational approach, the crudest approximation in which *all* couplings are disregarded provides a lower bound energy for the exact value. That is the extreme uncoupled adiabatic approximation (EUAA). This behavior can be summarized by the inequality[39,40]

$$E_{\text{EUAA}} \leqslant E_{\text{exact}} \leqslant E_{\text{CAA}} \leqslant E_{\text{UAA}}, \tag{13}$$

where the uncoupled adiabatic approximation (UAA) is the approximation where only the diagonal nonadiabatic coupling is taken into account. The efficiency of the HAA is evident by observing that in the simple EUAA the lowest potential curve gives rise to a bound energy. In conjunction with the second approach (UAA), which is also numerically simple, a well defined energy range is obtained, where the exact value is enclosed. The use of these two approaches is sufficient to predict the energy with an error of about 0.3% for the bound excitons considered in this paper. As more couplings are taken into account, the error drops as, for instance, for four coupled channels it will be of order of 0.01%. Another important characteristic is that the potential curves and nonadiabatic couplings are energy independent, which means that once calculated, all bound states and continuum solutions are obtained using Eq. (10) with proper boundary conditions.

III. SOLUTION OF THE ANGULAR EQUATION: POTENTIAL CURVES

The angular Eq. (9) contains all information about the particle interactions. Consequently, the efficiency of the hyperspherical adiabatic approach depends upon the determination of accurate potential curves and channel functions, which are used in the nonadiabatic couplings and radial equations. The establishment of precise angular solutions is not an easy task due to the different contributions of particle interactions in the angular equation as R changes.

At $R=0$ the potential vanishes and consequently the angular function is distributed along the whole range of the hyperangle α. For large values of R the angular functions are localized around $\alpha=0$, which corresponds to the wave function of the electron bound to the impurity center, forming a hydrogenic atom, and the scattered hole.

For small values of R the angular solution behavior is similar to the exact $R=0$ solution, given by the hyperspherical harmonics,

$$\Phi_{nl_el_h}(0;\Omega)=(\sin\alpha)^{l_e+1}(\cos\alpha)^{l_h+1}P_n^{l_e+1/2,l_h+1/2} \times(\cos 2\alpha)\mathcal{Y}^{LM}_{l_el_h}(\Omega_e,\Omega_h), \tag{14}$$

where $\mathcal{Y}^{LM}_{l_el_h}(\Omega_e,\Omega_h)$ are the coupled two-body spherical harmonics and l_e,l_h are the individual angular momentum quantum numbers of both electron and hole. The functions $P_n^{a,b}(z)$ are the Jacobi polynomials.[41] The exact eigenvalues of Eq. (9) at $R=0$ are calculated by

$$U_\mu(0)=-(l_e+l_h+2n+2)^2. \tag{15}$$

In the asymptotic limit ($R\to\infty$) the potential curves behave as[20,42]

$$-\frac{U_\mu(R)}{R^2}=-\frac{Z^2}{N_\mu^2}-\frac{2(Z-1)}{R}+\frac{U_\mu^{(2)}}{R^2}+\ldots, \tag{16}$$

where the parameter N_μ is the principal quantum number of the hydrogenic impurity-electron system. For the lowest potential curve ($\mu=1$), $U_1^{(2)}=L(L+1)-1/2$,[42] where L is the total angular momentum of the system.

An approach that has been used to obtain the angular solutions for other values of R is the diagonalization of the angular equation using the hyperspherical harmonics as basis functions.[38,25] However, this approach provides converged results only in the small-R region[43] and is very ineffective for mid- to large-R regions. Another approach is the direct numerical solution of the equations using methods such as the Numerov procedure,[44] with large scale numerical efforts involved. In this paper an analytical and very precise approach based on the expansion of the angular functions in power series of a new variable $x=\tan(\alpha/2)$ is used.[23] This variable transforms the angular equation with trigonometric

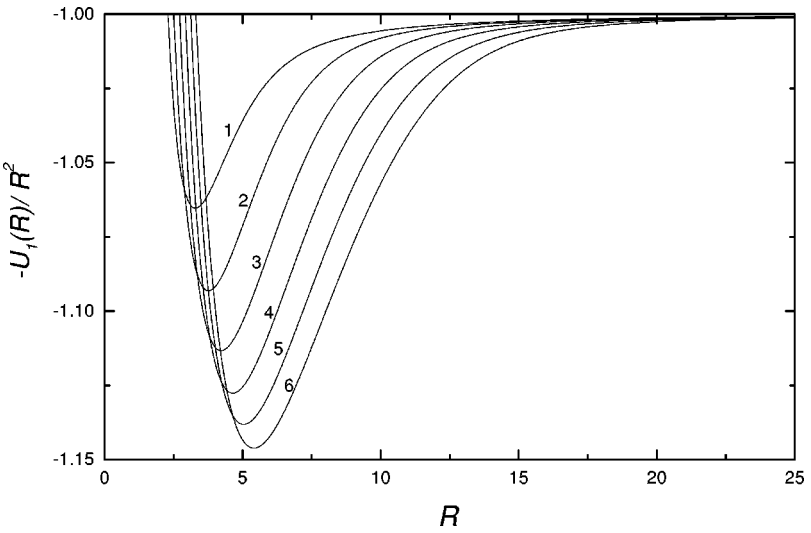

FIG. 1. The lowest potential curves for different values of $1/\sigma$ $(1,\ldots,6)$. The potential curves become deeper as the holes become heavier than the electrons, i.e., as $1/\sigma$ increases. For the masses shown in this work these potential curves hold only one binding energy, but as $\sigma=m_e/m_h$ becomes smaller, vibrational energies arise.

coefficients into an equation with rational coefficients, allowing the use of the Frobenius method. The resulting series convergence is very stable, precise, and numerically much faster than direct numerical methods. The angular function is then defined as

$$\Phi_\mu(R;\Omega)=\sum_{l_e l_h}(\sin\alpha)^{l_e+1}(\cos\alpha)^{l_h+1}e^{-ZR\alpha/N_\mu}\times G^L_{\mu l_e l_h}(R,\alpha)\mathcal{Y}^{LM}_{l_e l_h}(\Omega_e,\Omega_h), \tag{17}$$

where $\alpha=2\tan^{-1}(x)$. The exponential term is introduced to obtain the correct asymptotic behavior and depends on parameter N_μ. For small and large values of R the convergence of the channel function expansion in power series is very fast, which shows the importance of the analytical solution obtained from a single recurrence series.

The nonadiabatic couplings involve the first and second derivatives of the channel functions with respect to R, and consequently are very sensitive to any imprecision, especially sensitive when the potential curves approach to each other. With the procedure used in this work to build the channel functions, the nonadiabatic couplings become very stable. The $Q_{\mu\nu}(R)$'s, which involve second derivatives and are usually very small, are obtained numerically by standard five-point algorithms, but the $P_{\mu\nu}(R)$'s are calculated using the expression

$$P_{\mu\nu}(R)=-\frac{\langle\Phi_\mu|\hat{V}(\Omega)|\Phi_\nu\rangle}{U_\mu-U_\nu},\qquad U_\mu\neq U_\nu, \tag{18}$$

which is much less sensitive to numerical fluctuations than the one which uses numerical derivatives. With the potential curves and nonadiabatic couplings determined it is then possible to obtain the energy and the radial amplitudes $F_\mu(R)$ by solving the radial equation. The solutions are obtained starting the numerical propagation of the radial functions from the analytical solutions at $R\sim 0$, which involves logarithmic singularities,[45,46] and matching with the functions propagated from the asymptotic region, as described in Ref. 15.

IV. RESULTS

This section presents the binding energies for excitons bound to impurities for systems with $1\leqslant 1/\sigma\leqslant 6$. Initially the precision of potential curves and nonadiabatic couplings as well as the accuracy of binding energies are analyzed.

The ground-state solutions for the bound excitons are cal-

TABLE I. Convergence of the point of minimum for the lowest potential $U_\mu(R)/R^2$ $(\mu=1)$ as a function of $l_{\max}$ [see Eq. (17)], for each mass ratio $1/\sigma$ ranging from 1 to 6.

$l_{\max}\backslash 1/\sigma$	1	2	3	4	5	6
7	−1.064 508 1	−1.091 076 4	−1.109 996 3	−1.123 291 8	−1.132 988 3	−1.140 312 6
9	−1.064 890 7	−1.092 255 6	−1.111 888 2	−1.125 751 8	−1.135 891 8	−1.143 575 3
11	−1.065 071 1	−1.092 824 5	−1.112 810 4	−1.126 958 7	−1.137 325 9	−1.145 201 9
13	−1.065 166 6	−1.093 129 8	−1.113 308 7	−1.127 616 2	−1.138 118 2	−1.146 117 7
15	−1.065 165 6	−1.093 142 9	−1.113 341 9	−1.127 668 3	−1.138 187 2	−1.146 204 5
17	−1.065 168 4	−1.093 154 6	−1.113 363 2	−1.127 698 7	−1.138 226 8	−1.146 253 4
19	−1.065 169 5	−1.093 159 1	−1.113 371 4	−1.127 710 7	−1.138 243 2	−1.146 273 6
21	−1.065 169 9	−1.093 160 8	−1.113 374 4	−1.127 715 5	−1.138 249 9	−1.146 281 3
23	−1.065 170 0	−1.093 161 3	−1.113 375 4	−1.127 717 2	−1.138 252 3	−1.146 283 8

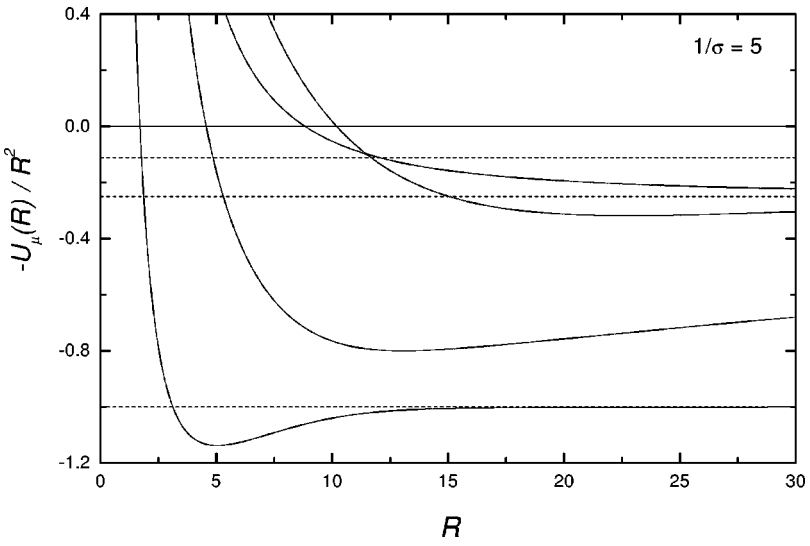

FIG. 2. The lowest four potential curves ($\mu=1,\ldots,4$ from bottom to top) for CdS semiconductor ($1/\sigma=5$) used in the calculation. Note the avoided-crossing region ($R\sim11.5$).

culated for total angular momentum $L=0$, which means that the individual angular momentum for the electron and hole are given by $l_e=l_h=l$. To obtain the angular solutions it is necessary to truncate the number of coupled components used in expansion (17) for the solution of the angular Eq. (9), defining a maximum value for $l=l_{\max}$. Figure 1 shows the lowest potential curves $U_1(R)$ divided by R^2 for different values of $1/\sigma$, using $l_{\max}=23$. The convergence of these curves can be analyzed at their point of minimum with respect to the value of $l_{\max}$, as listed in Table I. This table shows that a very good convergence for the minimum of the potential is achieved, which is the most difficult point to calculate. The first potential curve of each system is the most important one for our calculations since it contains the bound state energies. The remaining potential curves ($\mu=2,3,4$) were calculated using $l_{\max}=13$. This is an improvement of the calculation from Ref. 15 in which all potential curves have been calculated using $l_{\max}=13$. For small and large values of R the convergence is much faster, reflecting the appropriate choice of variable $x=\tan(\alpha/2)$ to expand the channel functions and the introduction of the exact $R=0$ and $R\rightarrow\infty$ behavior in expansion (17). One of the characteristics of these potential curves is the absence of vibrational levels. They support only a weak bound state, whose energy becomes smaller as σ approaches the critical mass. Figure 1 also shows that the potentials become deeper as the mass ratio $1/\sigma$ increases from 1 to 6, allowing larger binding energies.

For the CdS semiconductor, in which the hole is five times heavier than the electron,[9] the first four potential curves ($\mu=1,\ldots,4$) used in the calculation are shown in Fig. 2. Note the avoided-crossing region ($R\sim11.5$) between the curves with $\mu=3$ and $\mu=4$. In such region, the nonadiabatic couplings present peaks, where it is more difficult to calculate the channel functions. In practice, the peaks do not have a significative contribution for the calculation of the ground-state energy.

The hyperspherical adiabatic approach is appropriate for the energies calculation since R is a good adiabatic variable. This is reflected in the results shown in Table II, where the binding energy can be estimated qualitatively in the simplest radial equation approximation [EUAA result, cf. Eq. (13)], where all nonadiabatic couplings are disregarded. Aside from the numerical work to solve the angular equation [Eq. (9)] to obtain the potential curves, the energies are easily obtained from a single one-dimensional second order radial differential equation [Eq. (10)]. In Table II we also compare the calculated energy using the EUAA with our best, four coupled-channel calculation [CAA result, cf. Eq. (13)]. We see that the differences between our best values and the EUAA values are around only 1%, showing the accuracy of the method. For values of $1/\sigma<2.5$, there is not a binding energy in a coupled calculation, as we shall discuss further. A better result than the EUAA calculation is also obtained from a single differential equation, when the diagonal nonadiabatic coupling $Q_{11}(R)$ is taken into account [UAA result, cf. Eq. (13)]. These two approximations restrict with upper and lower bounds the region where the exact energy is found. To further improve the results the nondiagonal nonadiabatic

TABLE II. Comparison between the ground-state energy, obtained in the approximation where all nonadiabatic couplings are disregarded [EUAA result, cf. Eq. (13)], with our best coupled-channel calculation [CAA result, cf. Eq. (13)] in which it has been used for coupled radial equations. E_D is the donor ground-state energy.

$1/\sigma$	$(E_{\mathrm{EUAA}}-E_D)/E_D$ (%)	$(E_{\mathrm{EUAA}}-E_{\mathrm{CAA}})/E_{\mathrm{CAA}}$ (%)
1.0	0.075	
1.5	0.176	
2.0	0.509	
2.5	0.997	0.923
3.0	1.636	1.077
3.5	2.247	1.086
4.0	2.907	1.043
4.5	3.547	0.984
5.0	4.153	0.922
5.5	4.718	0.865
6.0	5.240	0.812

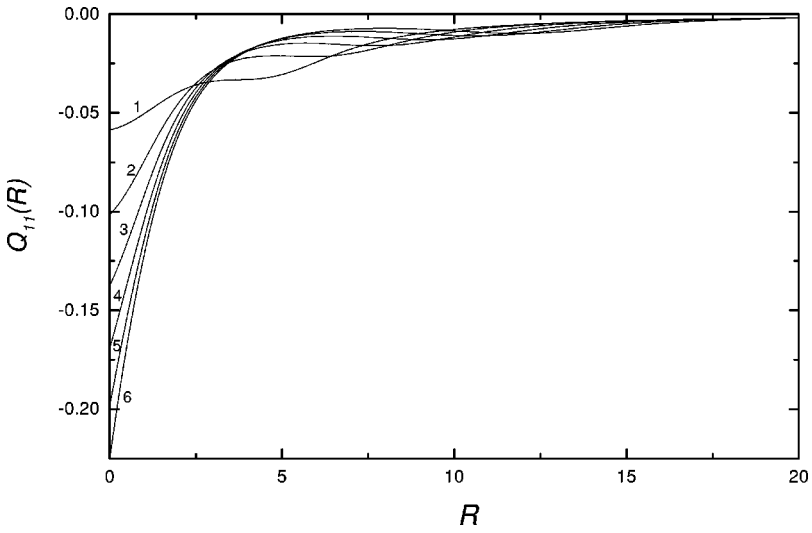

FIG. 3. Behavior of the diagonal nonadiabatic coupling $Q_{11}(R)$ for $1/\sigma=1,\ldots,6$ (from top to bottom, at the origin). The introduction of this function into the radial equation rises the lower bound energy obtained with only the first potential curve to an upper bound energy, which is much more precise.

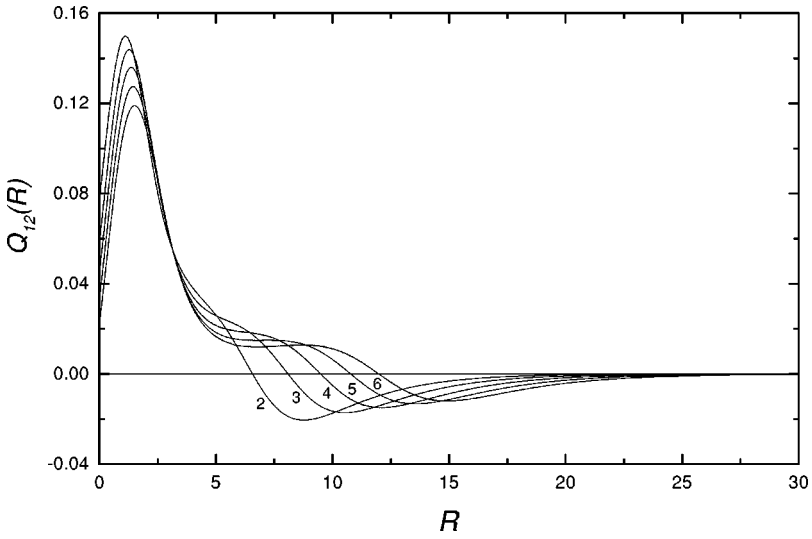

FIG. 4. Nonadiabatic couplings $Q_{12}(R)$ for the mass relation $1/\sigma=2,\ldots,6$ (from bottom to top, at the peak region). The nonadiabatic couplings $Q_{\mu\nu}(R)$ are the most difficult to be calculated as they involve the second derivative of the channel functions and demand the use of finite step derivatives. They are particularly unstable close to the avoided-crossing region of the potential curves.

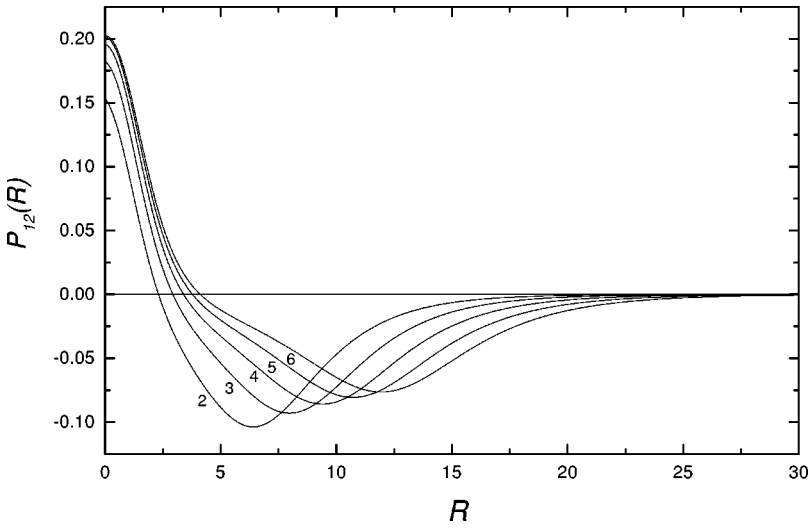

FIG. 5. The same as in Fig. 4 but for the $P_{12}(R)$ couplings. These couplings involve the first derivative of the angular channel, but they are calculated from the analytical expression given by Eq. (18).

TABLE III. Convergence of the ground-state energy $[(E-E_D)/E_D\ (\%)]$ as a function of number N_c of coupled radial equations [see Eq. (10)] for some representative values of the mass relation $1/\sigma$. Both EUAA and UAA calculations use a single uncoupled radial equation. The EUAA calculation (lower bound) neglects all nonadiabatic couplings while the UAA calculation (upper bound) only introduces the diagonal coupling $Q_{11}(R)$ [see Eq. (13)].

$N_c \backslash 1/\sigma$	2.5	3.0	3.5	4.0	4.5	5.0	5.5	6.0
1[a]	0.997	1.636	2.247	2.907	3.547	4.153	4.718	5.240
1[b]	0.039	0.461	1.032	1.717	2.409	3.076	3.702	4.282
2	0.056	0.510	1.095	1.786	2.479	3.143	3.764	4.339
3	0.071	0.546	1.140	1.835	2.529	3.192	3.812	4.386
4	0.074	0.553	1.149	1.844	2.538	3.201	3.820	4.392

[a]EUAA calculation.
[b]UAA calculation.

couplings were calculated and the coupled radial equation for up to four coupled radial components were solved. Some significative samples of the couplings are shown in Figs. 3–5. The resulting energies from this procedure are listed in Table III and also shown in Fig. 6, where one can see how the binding energy as a function of $1/\sigma$ converges as the number of coupled radial channel is increased. The highest curve in Fig. 6 corresponds to the calculation using the extreme uncoupled adiabatic approximation (EUAA), where only the potential curve $U_1(R)$ is considered in the radial equation. This curve defines a lower bound for the exact energy. The lowest curve represents the uncoupled approximation (UAA), which adds the nonadiabatic diagonal coupling $Q_{11}(R)$ to the lowest potential curve. As the nonadiabatic couplings are taken into account the curve rises toward the exact energies. An interesting behavior observed in this figure is how the energy decreases when $1/\sigma$ approaches the region of the critical mass. One could expect that the energy would reach zero quasilinearly if the energies of $1/\sigma \leqslant 3$ had not been calculated. In this case, the value for a critical mass

TABLE IV. Comparison between our estimated value for the critical mass $\sigma_{\rm crit}$ and those calculated by other authors. Our estimation has been done in the adiabatic, quasiseparable approximation (UAA).

Reference	$1/\sigma_{\rm crit}$
Present work	2.32
Jiang (Ref. 13)	2.94
Stébé and Stauffer (Ref. 47)	2.78
Skettrup *et al.* (Ref. 9)	2.35
Geltler *et al.* (Ref. 48)	0.75
Suffczynski *et al.* (Ref. 8)	3.0
Sharma and Rodriguez (Ref. 7)	5.0
Frost *et al.* (Ref. 49)	2.62
Hopfield (Ref. 5)	1.4

$\sigma_{\rm crit}$ around $1/\sigma_{\rm crit}=2.7$ could be prematurely estimated. Instead, the curve changes its curvature, which pushes the predicted critical mass to a smaller value of $1/\sigma_{\rm crit}$. Our estimation for $\sigma_{\rm crit}$ in the one-channel approximation (UAA) is close to $1/\sigma_{\rm crit}=2.32$. This behavior is shown in the inset of Fig. 6. Table IV shows the comparison between our estimated value for $\sigma_{\rm crit}$ and those of other references. Large discrepancies among different authors can be found, where the majority of the calculations is based upon variational techniques. Our value for $\sigma_{\rm crit}$ is best compared with that from Skettrup *et al.*,[9] which have added a long-range tail to their variational trial function.

In Ref. 9 Skettrup *et al.* have listed experimental data for CdS ($1/\sigma=5$) and ZnO ($1/\sigma=4.762$). For CdS, the experimental value for the difference between the bound-state energy (E) and the binding energy of the free exciton ($E_{\rm ex}$) ranges from 4.66–7.10 meV. Their computed value for $E-E_{\rm ex}$ is 6.4 meV which compares with our best four coupled-channel calculation result of 6.437 meV. For ZnO, $E-E_{\rm ex}=14.3$ meV which is compared with our value of 14.453 meV. According to Ref. 9, the experimental value for ZnO ranges from 11.3 to 20.9 meV.

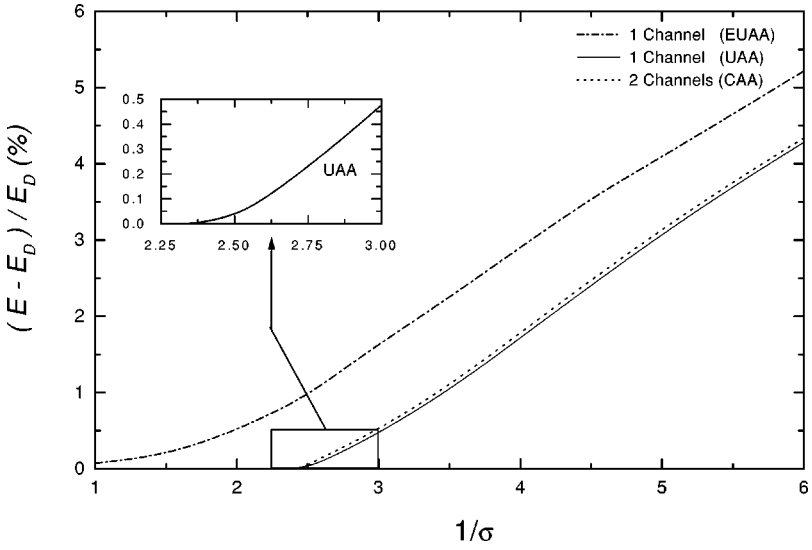

FIG. 6. Energy of excitons bound to an impurity donor as a function of the relative electron-hole mass. The highest and lowest curves are the EUAA and UAA calculations, respectively. The other curve is a CAA calculation. In the inset one can see the curvature change for the UAA calculation, whose estimation for $1/\sigma_{\rm crit}=2.32$.

V. CONCLUSIONS

The adiabatic approach using hyperspherical coordinates has proved to be a precise, intuitive, and elegant procedure to analyze the weak binding energies of excitons bound to impurity donor centers. An important aspect of the hyperspherical adiabatic approach is: as the nonadiabatic couplings are introduced into the radial equations, the energy approaches the exact value. A demonstration of the appropriateness of the method is the determination of the energy using the simplest one potential curve approximation, with an error of only 1%, which is usually a good value for such solid-state excitonlike approximated systems. The precision was further improved by the inclusion of up to four potential curves and the corresponding nonadiabatic couplings in the radial equations. The resulting energies can be compared with the most accurate variational results. One of the objectives of using high-precision calculation is to make possible a better analysis of the critical mass region.

This paper presented the calculations of the binding energies of excitons bound to impurity donors for holes with six times the electron effective mass up to systems where σ is close to the critical values. This treatment is a good alternative to the adiabatic molecular approaches, which are inappropriate due to the small mass of the hole. The HAA is an *ab initio* approach and uses the potential curve picture to locate the energies. It is more practical than a variational approach, especially considering that compared with the results in literature, the results presented here have comparable precision and accuracy.

The improvement of our result for σ_{crit} demands a much more elaborated numerical work since the energy is very small. Nevertheless, such precision is not meaningful from a solid-state point of view since the errors of the effective-mass approximation are much more significant. Anyhow this is an interesting theoretical problem which may be better analyzed in more detailed studies.

ACKNOWLEDGMENTS

The authors would like to thank Fundação de Amparo à Pesquisa do Estado de São Paulo (FAPESP, Brazil) for the financial support, under Processes No. 97/06271-1 and No. 99/11363-8. A.S.S. would also like to acknowledge the financial support from CNPq and Capes (Brazilian agencies).

[1] M.A. Lampert, Phys. Rev. Lett. **1**, 450 (1958).
[2] J.R. Haynes, Phys. Rev. Lett. **4**, 361 (1960).
[3] D.G. Thomas and J.J. Hopfield, Phys. Rev. Lett. **5**, 505 (1960).
[4] D.G. Thomas and J.J. Hopfield, Phys. Rev. **128**, 2135 (1962).
[5] J. J. Hopfield, in *Proceedings of the Seventh International Conference on the Physics of Semiconductors, Paris, 1964*, edited by M. Hulin (Dundod, Paris, 1964), p. 725.
[6] Y.S. Park, C.W. Litton, T.C. Collins, and D.C. Reynolds, Phys. Rev. **143**, 512 (1966).
[7] R.R. Sharma and S. Rodriguez, Phys. Rev. **153**, 823 (1967).
[8] M. Suffczynski, W. Gorzkowski, and R. Kowalczyk, Phys. Lett. **24A**, 453 (1967).
[9] T. Skettrup, M. Suffczynski, and W. Gorzkowski, Phys. Rev. B **4**, 512 (1971).
[10] S.G. Elkomoss and A.S. Amer, Phys. Rev. B **11**, 2222 (1975).
[11] M. Suffczynski and L. Wolniewicz, Phys. Rev. B **40**, 6250 (1989).
[12] A.C. Cancio and Y.-C. Chang, Phys. Rev. B **47**, 13 246 (1993).
[13] T.-F. Jiang, Solid State Commun. **74**, 899 (1990).
[14] J.J. De Groote, J.E. Hornos, H.T. Coelho, and C.D. Caldwell, Phys. Rev. B **46**, 2101 (1992).
[15] J.J. De Groote, A.S. dos Santos, M. Masili, and J.E. Hornos, Phys. Rev. B **58**, 10 383 (1998).
[16] M. Masili, J.E. Hornos, and J.J. De Groote, Phys. Rev. A **52**, 3362 (1995).
[17] J.J. De Groote, M. Masili, and J.E. Hornos, J. Phys. B **31**, 4755 (1998).
[18] M. Masili, J.J. De Groote, and J.E. Hornos, J. Phys. B **33**, 2641 (2000).
[19] J.J. De Groote, M. Masili, and J.E. Hornos, Phys. Rev. A **62**, 032508 (2000).
[20] J.H. Macek, J. Phys. B **1**, 831 (1968).
[21] U. Fano, Phys. Today **29**(9), 32 (1976).
[22] C.H. Greene, Phys. Rev. A **23**, 661 (1981).
[23] J.E. Hornos, S.W. MacDowell, and C.D. Caldwell, Phys. Rev. A **33**, 2212 (1986).
[24] H.T. Coelho, J.J. De Groote, and J.E. Hornos, Phys. Rev. A **46**, 5443 (1992).
[25] C.D. Lin, Phys. Rep. **257**, 1 (1995), and references therein.
[26] C.D. Lin and X.H. Liu, Phys. Rev. A **37**, 2749 (1988).
[27] J.Z. Tang, S. Watanabe, and M. Matsuzawa, Phys. Rev. A **46**, 2437 (1992).
[28] C.W. Clark and C.H. Greene, Phys. Rev. A **21**, 1786 (1980).
[29] C.H. Greene and C.W. Clark, Phys. Rev. A **30**, 2161 (1984).
[30] C.H. Greene, Phys. Rev. A **22**, 149 (1986).
[31] C.G. Bao and C.D. Lin, Few-Body Syst. **16**, 47 (1994).
[32] X. Yang, J. Xi, C.G. Bao, and C.D. Lin, Phys. Rev. A **52**, 2029 (1995).
[33] X. Yang, C.G. Bao, and C.D. Lin, Phys. Rev. Lett. **76**, 3096 (1996).
[34] T. Morishita, O.I. Tolstikhin, S. Watanabe, and M. Matsuzawa, Phys. Rev. A **56**, 3559 (1997).
[35] T. Morishita and C.D. Lin, J. Phys. B **31**, L209 (1998).
[36] T. Morishita and C.D. Lin, Phys. Rev. A **57**, 4268 (1998).
[37] T. Morishita and C.D. Lin, Phys. Rev. A **59**, 1835 (1999).
[38] Yu.F. Smirnov and K.V. Shitikova, Fiz. Elem. Chastits At. Yadra **8**, 847 (1977) [Sov. J. Part. Nucl. **8**, 344 (1977)].
[39] A.F. Starace and G.L. Webster, Phys. Rev. A **19**, 1629 (1979).
[40] H.T. Coelho and J.E. Hornos, Phys. Rev. A **43**, 6379 (1991).
[41] *Handbook of Mathematical Functions*, 3rd ed., edited by M. Abramowitz and I. A. Stegun (Dover, New York, 1965).
[42] Z. Zhen and J. Macek, Phys. Rev. A **34**, 838 (1986).
[43] T.K. Das, R. Chattopadhyay, and P.K. Mukherjee, Phys. Rev. A **50**, 3521 (1994).

[44] Y.D. Wang and J. Callaway, Phys. Rev. A **48**, 2058 (1993).
[45] J.H. Bartlett, Phys. Rev. **51**, 661 (1937).
[46] V.A. Fock, Izv. Akad. Nauk SSSR, Ser. Fiz. **18**, 161 (1954).
[47] B. Stébé and L. Stauffer, in *Proceedings of the Fourth International Conference on Superlattices, Microstructures, and Microdevices, Trieste, 1988.*
[48] T.H. Geltler, H.B. Snodgrass, and L. Spruch, Phys. Rev. **172**, 110 (1968).
[49] A.A. Frost, M. Inokuti, and J.P. Lowe, J. Chem. Phys. **41**, 482 (1964).